Li et al. *Zool. Res.* 2024, 45(5): 990−1000
https://doi.org/10.24272/j.issn.2095-8137.2023.392
https://cstr.cn/32248.14.zr.2024.392

ZR | Zoological Research

Article Open Access

Mandarin fish von Hippel-Lindau protein regulates the NF-κB signaling pathway via interaction with IκB to promote fish ranavirus replication

Zhi-Min Li[1], Xiao-Wei Qin[1], Qi Zhang[1], Jian He[1], Min-Cong Liang[1], Chuan-Rui Li[1], Yang Yu[1], Weng-Hui Liu[1], Shao-Ping Weng[1], Jian-Guo He[1,*], Chang-Jun Guo[1,2,*]

[1] *School of Marine Sciences*, *State Key Laboratory for Biocontrol*, *Southern Marine Science and Engineering Guangdong Laboratory (Zhuhai)*, *Guangdong Province Key Laboratory of Aquatic Economic Animals* & *Guangdong Provincial Observation and Research Station for Marine Ranching of the Lingdingyang Bay*, *Sun Yat-sen University*, *Guangzhou*, *Guangdong* 510275, *China*

[2] *Guangdong Laboratory for Lingnan Modern Agriculture*, *South China Agricultural University*, *Guangzhou*, *Guangdong* 510640, *China*

ABSTRACT

The von Hippel-Lindau tumor suppressor protein (VHL), an E3 ubiquitin ligase, functions as a critical regulator of the oxygen-sensing pathway for targeting hypoxia-inducible factors. Recent evidence suggests that mammalian VHL may also be critical to the NF-κB signaling pathway, although the specific molecular mechanisms remain unclear. Herein, the roles of mandarin fish (*Siniperca chuatsi*) VHL (*sc*VHL) in the NF-κB signaling pathway and mandarin fish ranavirus (MRV) replication were explored. The transcription of *sc*VHL was induced by immune stimulation and MRV infection, indicating a potential role in innate immunity. Dual-luciferase reporter gene assays and reverse transcription quantitative PCR (RT-qPCR) results demonstrated that *sc*VHL evoked and positively regulated the NF-κB signaling pathway. Treatment with NF-κB signaling pathway inhibitors indicated that the role of *sc*VHL may be mediated through *sc*IKKα, *sc*IKKβ, *sc*IκBα, or *sc*p65. Co-immunoprecipitation (Co-IP) analysis identified *sc*IκBα as a novel target protein of *sc*VHL. Moreover, *sc*VHL targeted *sc*IκBα to catalyze the formation of K63-linked polyubiquitin chains to activate the NF-κB signaling pathway. Following MRV infection, NF-κB signaling remained activated, which, in turn, promoted MRV replication. These findings suggest that *sc*VHL not only positively regulates NF-κB but also significantly enhances MRV replication. This study reveals a novel function of *sc*VHL in NF-κB signaling and viral infection in fish.

This is an open-access article distributed under the terms of the Creative Commons Attribution Non-Commercial License (http://creativecommons.org/licenses/by-nc/4.0/), which permits unrestricted non-commercial use, distribution, and reproduction in any medium, provided the original work is properly cited.

Copyright ©2024 Editorial Office of Zoological Research, Kunming Institute of Zoology, Chinese Academy of Sciences

Keywords: VHL; NF-κB; IκBα; Ranavirus; Mandarin fish

INTRODUCTION

As an E3 ubiquitin ligase, the von Hippel-Lindau tumor suppressor protein (VHL) functions as a critical regulator of the oxygen-sensing pathway, targeting hypoxia-inducible factors (HIFs) (Bader & Hsu, 2012). Mammalian VHL (pVHL) also participates in various HIF-independent activities, serving as a multipurpose adaptor protein that regulates a wide variety of transcription-dependent and transcription-independent cellular processes, including cell division, apoptosis, differentiation, and extracellular matrix formation (Barontini & Dahia, 2010; Gossage et al., 2015; Hudler & Urbancic, 2022). Recent evidence has indicated that pVHL plays important roles in the NF-κB signaling pathway. Notably, pVHL can interact with IKKα and IKKβ, mediating K63-linked ubiquitination of IKKβ to inhibit its activation (Wang et al., 2016). In pVHL-defective clear-cell renal cell carcinoma, loss of pVHL induces a mesenchymal transition largely dependent on HIF-1α-induced NF-κB (An & Rettig, 2005; Pantuck et al., 2010), while increased pVHL expression is accompanied by elevated mRNA levels of NF-κB and kinases PDK1 and Akt in patients with disseminated forms of the disease (Spirina et al., 2019). Despite these observations, the molecular mechanisms by which VHL regulates NF-κB activation remain unclear.

Received: 18 April 2024; Accepted: 30 April 2024; Online: 01 May 2024

Foundation items: This work was supported by the National Key Research and Development Program of China (2022YFE0203900), Guangdong Key Research and Development Program (2021B0202040002 and 2022B1111030001), China Agriculture Research System (CARS-46), Guangdong Basic and Applied Basic Research Foundation (2021A1515010647), Basic and Applied Basic Research Project of Guangzhou Science and Technology Plan Project (202102020299), Science and Technology Planning Project of Guangdong (2023B1212060023), and Guangdong Laboratory for Lingnan Modern Agriculture (NZ2021018)

*Corresponding authors, E-mail: gchangj@mail.sysu.edu.cn; lsshjg@mail.sysu.edu.cn

The mandarin fish (*Siniperca chuatsi*), a species belonging to Perciformes, is widely distributed in China and holds considerable economic value in the aquarium trade (He et al., 2020). Due to intensive aquaculture practices aimed at meeting the human demand for animal protein, high-density farming of mandarin fish is frequently threatened by disease outbreaks, especially the Mandarin fish ranavirus (MRV) (Dong et al., 2017; He et al., 1998, 2000). MRV, a double-stranded DNA (dsDNA) virus within the *Iridoviridae* family, *Alphairidovirinae* subfamily, and *Ranavirus* genus (Dong et al., 2017), is a novel and lethal mandarin fish pathogen responsible for substantial economic losses in China (Zhang et al., 2020). However, the pathogenic mechanisms of MRV and its interactions with the host immune system remain largely unexplored.

In the present study, the molecular mechanisms by which *S. chuatsi* VHL (*sc*VHL) positively regulates the NF-κB signaling pathway and promotes MRV replication were investigated.

MATERIALS AND METHODS

Fish, cell line, and virus

Healthy mandarin fish (average body weight ±30 g and size ±10 cm) were purchased from Nanhai Aquafarm and acclimatized in laboratory aquarium tanks at 28°C for one week prior to experimentation. All animal procedures were performed in accordance with the regulations for animal experimentation in Guangdong Province, China, and permitted by the Ethics Committee of Sun Yat-sen University (no. 2019121705). The mandarin fish fry (MFF-1) cell line, developed and characterized in our laboratory, was cultured as a monolayer in Dulbecco's modified Eagle's medium (DMEM) supplemented with 10% fetal bovine serum (FBS, Invitrogen-Gibco, USA) at 27°C in a 5% CO_2 incubator (Dong et al., 2008). Fathead minnow (FHM) cells (ATCC CCL-42) were maintained in M199 medium supplemented with 10% FBS (Invitrogen-Gibco, USA) at 27°C (Luo et al., 2023). The NH-1609 MRV strain was originally isolated from moribund hybrid mandarin fish in Naihai, Guangdong, China, and preserved in our laboratory (Qin et al., 2023).

Sequence analysis

The sequences were analyzed using the Basic Local Alignment Search Tool (BLAST) from the National Center for Biotechnology Information (NCBI) website (http://www.ncbi.nlm.nih.gov/blast). The three-dimensional (3D) structure of the *sc*VHL protein was predicted by homology modeling in AlphaFold v.2.3.0. Amino acid alignments were performed using the ClustalX program and edited with GeneDoc v.2.7.0 software. The phylogenetic tree of VHL sequences was constructed using the neighbor-joining method in Molecular Evolutionary Genetics Analysis (MEGA) v.10.0 (Kumar et al., 1994), with reliability assessed with 1 000 bootstrap replicates.

Plasmid construction and cell transfection

*sc*VHL was constructed by polymerase chain reaction (PCR) and subsequently cloned and inserted into the pCMV-Myc-N (Takara, Japan), pCMV-HA-N (Takara, Japan), and pEGFP-N3 (Clontech, Japan) vectors to generate pCMV-*sc*VHL-Myc, pCMV-*sc*VHL-HA, and pEGFP-*sc*VHL plasmids, respectively. Furthermore, *sc*IKKα, *sc*IKKβ, *sc*IκBα, *sc*p65, *sc*p100, *sc*p105, *sc*c-Rel, *sc*Rel B, *sc*MyD88, and *sc*TNF-α were cloned and inserted into pCMV-Myc-N to generate Myc-tagged expression plasmids. Both *sc*IκBα and *sc*p65 were also constructed into expression plasmids tagged with HA and Flag. Various ubiquitin (Ub) constructs, including Ub-HA, Ub-K6-HA, Ub-K11-HA, Ub-K27-HA, Ub-K27R-HA, Ub-K29-HA, Ub-K33-HA, Ub-K48-HA, Ub-K48R-HA, and Ub-K63-HA, were synthesized by Beijing Qinke Technology (China). The primers with restriction enzyme sites used for gene cloning are listed in Supplementary Table S1. The plasmids were transfected into FHM cells using Fugene HD (Promega, USA) and MFF-1 cells using Transfect EZ 3000 Plus (eLGbio, China) following the manufacturers' standard protocols.

Antibodies and reagents

Primary antibodies included anti-β-actin (Proteintech, USA), anti-β-tubulin (1:5000, Proteintech, USA), anti-GFP (1:1000, Abcam, UK), anti-HA tag (1:1000, CST, USA), anti-Flag (1:1000, CST, USA), and anti-Myc (1:5000, Sigma, USA), and secondary antibodies included horseradish peroxidase (HRP)-goat-anti-mouse IgG (H+L) (1:5000, Promega, USA), (HRP)-goat-anti-rabbit IgG (H+L) (1:5000, Promega, USA). The proteasome inhibitor MG132, cycloheximide (CHX), phorbol 12-myristate 13-acetate (PMA), VH298, VH032, BAY11-7082, -(-)DHMEQ, ST 2825, and resatorvid were purchased from MCE (USA). Polyinosinic-polycytidylic acid (poly (I:C)) and lipopolysaccharides (LPS) were obtained from InvivoGen (France). Iodoacetamide (IAA) was purchased from Cell Signaling Technology (USA).

Western blot analysis

Cells were harvested and lysed with cell lysis buffer for western blotting and immunoprecipitation (IP, Beyotime, China) with a protease inhibitor cocktail (Merck Millipore, USA). The lysates were diluted with 5×sodium dodecyl sulfate (SDS) loading buffer and boiled for 10 min. Equal amounts of extracted protein were subjected to 10% SDS-polyacrylamide gel electrophoresis (SDS-PAGE) and transferred to a membrane probed with a specific antibody. Protein bands were detected using High-sig ECL western blotting substrate (Tanon, China) and visualized using the Amersham Image Quant 800 system (Cytiva, USA).

Co-immunoprecipitation (Co-IP) assay

For Co-IP analysis, FHM cells were seeded in 25 cm^2 dishes overnight and cotransfected with 2 μg of vector. At 24 h post-transfection, the medium was carefully removed, and the cells were lysed with IP lysis buffer (Beyotime, China) and protease inhibitor cocktail III (Merck Millipore, USA). Whole-cell lysates were subjected to centrifugation at 12 000 ×*g* for 10 min at 4°C, with the resulting supernatants collected for IP using Dynabeads Pierce protein G magnetic beads (Thermo Fisher, USA) according to the manufacturer's instructions. Briefly, the cell lysates were incubated with beads for 10 min at room temperature, after which the beads were removed. The supernatants were then incubated with anti-Myc (anti-HA) antibody for 30 min and with Dynabeads for 10 min at room temperature. After washing three times with IP washing buffer, the Dynabeads-antibody-antigen complex was gently resuspended with elution buffer and neutralization solution and analyzed by western blotting.

Dual-luciferase reporter system

FHM cells were cultured in 24-well plates and subsequently co-transfected with pRL-TK and ISRE-Luc/cGAS-Luc/STAT3-Luc/IFN-β-Luc/NF-κB-Luc plasmids (Promega, USA) along with the indicated plasmids or empty vector. After transfection,

the cells were treated with poly (I:C) (2 μg/mL) for 6 h or left untreated. Luciferase activity was measured using a Dual-Luciferase Reporter Gene Assay Kit (Promega, USA). Each independent experiment was performed in triplicate with three technical replicates. Luciferase activity was normalized to *Renilla* luciferase activity.

RNA extraction and reverse transcription quantitative PCR (RT-qPCR) analysis

Total RNA from cells or tissues was extracted using an SV Total RNA Isolation Kit (Promega, USA) and reverse transcribed using an Evo M-MLV qPCR RT Kit (AG, China) to synthesize first-strand cDNA according to the manufacturers' protocols. Analysis was performed with a Roche LightCycler® 480 instrument (Roche, Switzerland) using a SYBR Green Pro Taq HS Real-Time qPCR Kit (AG, China). Briefly, each assay was carried out in triplicate using the following cycling conditions: 95°C for 1 min for initial denaturation, followed by 40 cycles at 95°C for 15 s, 60°C for 15 s, and 72°C for 45 s. The expression levels of immune-related genes and viral genes were normalized to the expression of the *scβ-actin* gene. The primer sets for the *scVHL*, *scβ-actin*, *MRV-MCP*, *MRV-ICP18*, and *MRV-DNA polymerase* genes are described in Supplementary Table S2.

DNA extraction and virus load analysis

Total viral genomic DNA was extracted using a DNA isolation Mini Kit (Vazyme, China). Viral copies were analyzed via absolute quantitative real-time PCR (qPCR). Amplification and analysis were performed using a Roche LightCycler® 480 instrument and TaqMan Real PCR Easy™ Mix (FOREGENE, China) with specific primers and probes designed from the *MRV-MCP* sequence. Forward primer 5'-GTTACGGGTT CTGGCATCACTAG-3', reverse primer 5'-TTTCCACCGTAC AGCGCTTT-3', and probe 5'-FAM-TTCATTGATCTCGCCA CTTA-BHQ1-3' were identified. Each assay was carried out in triplicate with a 10 μL mixture containing 5 μL of TaqMan Real PCR Easy™ Mix, 200 nmol/L probe, 400 nmol/L primer each, and 100 ng of total DNA template. The program started at 94°C for 3 min for activation, followed by 45 cycles at 94°C for 10 s and 60°C for 30 s (Qin et al., 2023). Viral genomic copies were quantified by the amount of viral major capsid protein (*mcp*) gene copies, normalized to the standard curve (Luo et al., 2023).

Viral titer determination

Cells were transfected with different expression vectors, then collected 72 h post-MRV infection. MRV viral titers were measured in MFF-1 cells based on $TCID_{50}$ using a limiting dilution assay and calculated as described previously (Reed & Muench, 1938; Zeng et al., 2021).

Small interfering RNA (siRNA) assay

For siRNA transfections, Lipofectamine™ RNAiMAX (Invitrogen, USA) was used. MFF-1 cells were directly seeded in six-well cell culture plates the day before transfection. Approximately 5 μL of Lipofectamine™ RNAiMAX and diluted si-*sc*IκBα (5'-CCCTCCAGATGATCAAACT-3') and si-*sc*VHL (5'-GCTACATTTGCTAATATCA-3') were gently mixed with Opti-MEM (Gibco, USA) and incubated for 15 min at room temperature. Control siRNA (siRNA-NC) was obtained from Guangzhou RiboBio (China).

Statistical analysis

All statistical analyses were carried out using SPSS v.20 with one-way analysis of variance (ANOVA). Data are presented as mean±standard deviation (SD) from three independent experiments conducted in triplicate. Significance was determined at **: $P<0.01$ and *: $P<0.05$ compared to the controls.

RESULTS

Molecular characteristics of *sc*VHL

To investigate the molecular characteristics of VHL in mandarin fish, the coding sequence of *sc*VHL was analyzed and cloned from the mandarin fish genome (Gene ID: 10434). The *sc*VHL cDNA (XM_044177203) was 1 916 bp in length, including a 5'-untranslated region (UTR) of 307 bp, a 3'-terminal UTR of 1 105 bp, and an open reading frame (ORF) of 504 bp, encoding a 167 amino acid (aa) protein. Domain prediction analysis using BLAST and SMART indicated that *sc*VHL contained a VHL beta domain and VHL short C-terminal helical domain (Figure 1A). The 3D structure of *sc*VHL closely resembled that of *Danio rerio*, *Mus musculus*, and *Homo sapiens* (Figure 1B). Phylogenetic analysis showed that *sc*VHL clustered within the fish clade (Figure 1C), suggesting a close evolutionary relationship between teleost fish VHLs and mammalian VHLs. Identity and similarity analyses showed that *sc*VHL was most closely related to *Chelmon rostratus*, with 88.02% identity, followed by *Acanthopagrus latus* with 86.23% identity. These findings suggest that *sc*VHL shares a similar structure with VHL proteins from other species.

Expression patterns of scVHL in healthy fish and immune-stimulated MFF-1 cells

To investigate the tissue distribution of *sc*VHL mRNA, the expression levels of *sc*VHL across various tissues in healthy mandarin fish were determined. Results showed that the *scVHL* gene was widely expressed in the liver, gill, fat, brain, fin, spleen, heart, blood, intestine, hind kidney, middle kidney, head kidney, and muscle. Notably, *scVHL* expression was highest in the liver, approximately nine times higher than in the heart, followed by the brain and hind kidney, nearly six times higher than in the heart (Figure 1D). Given the importance of the liver and hind kidney as key immune tissues in teleost fish, the high expression of *scVHL* in these tissues suggests a potential role in the immune response of mandarin fish.

To investigate the involvement of *sc*VHL in immune responses, the expression patterns of *sc*VHL following immune stimulation were detected. Cells were stimulated with poly (I:C) (2 μg/mL), LPS (2 mg/mL), or PMA (10 μmol/L), with the mRNA expression level of *scVHL* subsequently determined via RT-qPCR. Results showed that *scVHL* was up-regulated in response to poly (I:C) and LPS stimulation (Figure 1E). Furthermore, the expression levels of *scVHL* mRNA after MRV infection *in vitro* and *in vivo* were further investigated. In the MFF-1 cells, *scVHL* expression was correlated with MRV infection and increased in a time-dependent manner, showing 10-, 100-, and 300-fold up-regulation at 36, 48, and 72 h post-infection, respectively (Figure 1F). Similarly, *scVHL* mRNA levels in the spleen were up-regulated 3-fold following MRV infection (Figure 1G). These findings indicate that *sc*VHL is responsive to immune stimuli and may play an important role in the innate immunity of mandarin fish.

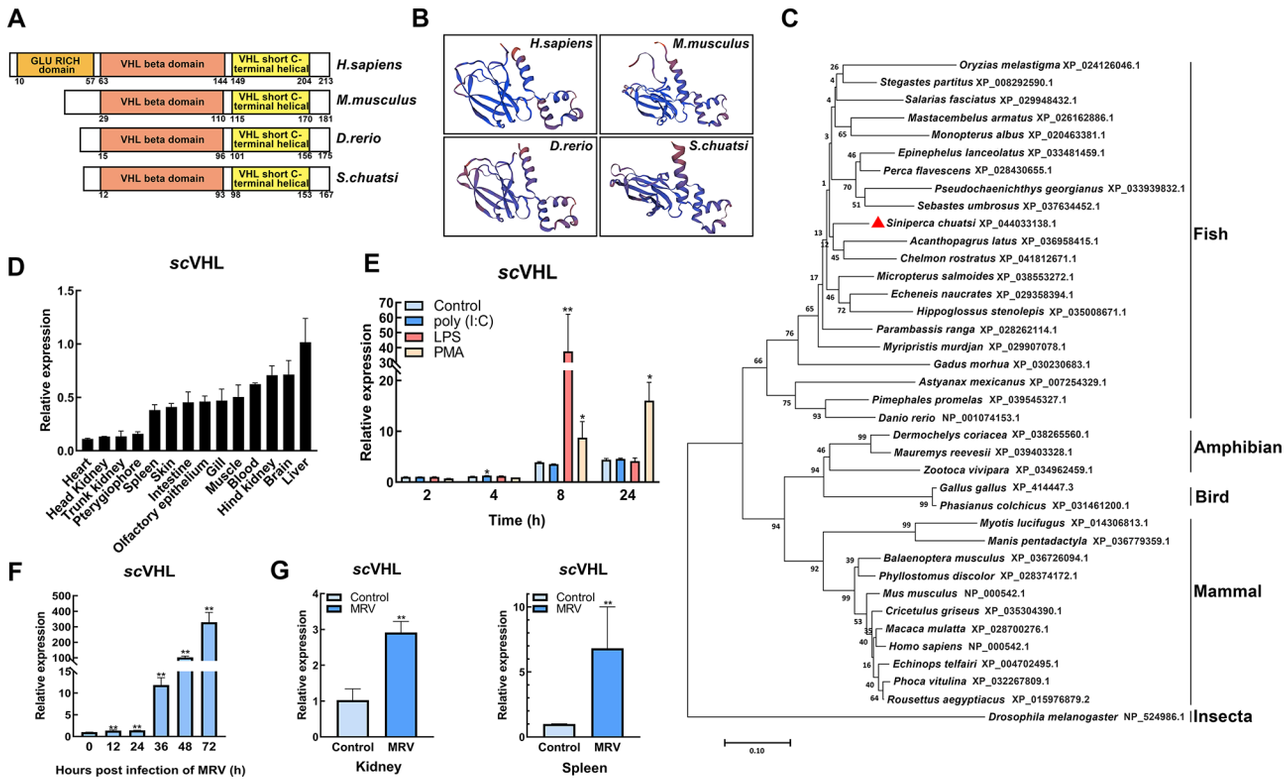

Figure 1 Characteristics of mandarin fish *sc*VHL

A, B: Comparison of motifs and domain structure of *sc*VHL protein. A: Numbers indicate positions of amino acid residues in each sequence. B: *sc*VHL protein structure was predicted using the Swiss model. Sequences used for comparison included *H. sapiens* (NP_000542.1), *M. musculus* (NP_033533.1), and *D. rerio* (NP_001074153.1). C: Phylogenetic tree constructed based on protein sequences of *scVHL* genes from different species using the neighbor-joining method with MEGA v.10 and 1 000 bootstrap replicates. D: Expression levels of *scVHL* in various mandarin fish tissues. E: Expression pattern of *scVHL* under immune stimulation. Transcription level of *scVHL* in MFF-1 cells under poly (I:C), LPS, and PMA stimulation. F, G: Expression of *scVHL* in response to virus. F: *scVHL* mRNA levels in MFF-1 cells were measured by RT-qPCR and normalized to the reference *β-actin* gene after infection with MRV at 0.1 MOI. G: *scVHL* mRNA levels were measured in mandarin fish kidney and spleen tissue after MRV infection. *: $P<0.05$; **: $P<0.01$.

*Sc*VHL evoked NF-κB signaling pathway activation

To explore the functional role of *sc*VHL in the innate immune response, dual-luciferase reporter gene assays were conducted. As depicted in Figure 2A, the relative level of NF-κB-luciferin showed a significant 12-fold increase after *sc*VHL overexpression, whereas the relative levels of ISRE-, GAS-, STAT3-, and IFN-β-luciferin remained unchanged compared to the control group. NF-κB-luciferin activity was induced by the increased *sc*VHL in a dose-dependent manner (Figure 2B). Furthermore, both the N-terminal domain (*sc*VHL-1, 1–93 aa) and C-terminal domain (*sc*VHL-2, 94–167 aa) of *sc*VHL significantly induced NF-κB-luciferin activity (Figure 2C). To determine whether functionally inactivated *sc*VHL could activate the NF-κB promoter, cells were treated with the VHL inhibitors VH298 (50 μmol/L) and VH032 (250 μmol/L) after co-transfection with *sc*VHL, NF-κB-Luc, and pRL-TK plasmids. As shown in Figure 2D, NF-κB-luciferin activity induced by *sc*VHL was markedly reduced after cells were treated with VH298 and VH032. To further confirm these findings, *sc*VHL vectors were overexpressed in MFF-1 cells, and the transcription of NF-κB target genes (*scTNF-α*, *scIL-1β*, and *scIL-18*) was detected via RT-qPCR at 24 h post-transfection. The expression levels of *scTNF-α*, *scIL-1β*, and *scIL-18* were significantly higher in *sc*VHL-Myc-overexpressing cells compared to control cells. These results indicate that *sc*VHL can activate and positively regulate the NF-κB signaling pathway.

*Sc*VHL interacted with *sc*IKKα, *sc*IKKβ, and *sc*IκBα

To determine the stage at which *sc*VHL affects NF-κB signaling, several pathway inhibitors were used, including BAY11-7082 (IκB kinase inhibitor), -(-)DHMEQ (NF-κB inhibitor), resatorvid (TNF-α and IL-6 inhibitor), and ST 2825 (IRAK1/4 inhibitor). Cells were co-transfected with *sc*VHL and NF-κB reporter plasmids. At 24 h post-transfection, the inhibitors were incubated with cells for 8 h, and promoter activation was detected via dual-luciferase reporter assays. As shown in Figure 2F, scVHL-induced NF-κB-luciferase activity was markedly inhibited by BAY11-7082, -(-)DHMEQ, and ST 2825, but not by resatorvid, suggesting that *sc*VHL targets *sc*IKKα, *sc*IKKβ, *sc*IκBα, or *sc*p65 in the NF-κB signaling pathway.

Co-IP analysis was performed to confirm these interactions. Results demonstrated that *sc*VHL co-precipitated with the *sc*IKKα (Figure 2G), *sc*IKKβ (Figure 2H), and *sc*IκBα proteins (Figure 2I), but showed no significant interaction with *sc*p65 (Figure 2J). Previous studies have indicated that pVHL interacts with IKKα and IKKβ and regulates K63-linked ubiquitination of IKKβ (Wang et al., 2016). Therefore, the interaction between *sc*VHL and *sc*IκBα was further explored. To identify key interaction sites between *sc*VHL and *sc*IκBα, *sc*VHL was divided into two segments: *sc*VHL-1 (1–93 aa), containing the β domain, and *sc*VHL-2 (94–167 aa), containing the α domain. Similarly, *sc*IκBα was divided into three segments: *sc*IκBα-ΔN (75–308 aa), *sc*IκBα-ΔANK (1–74

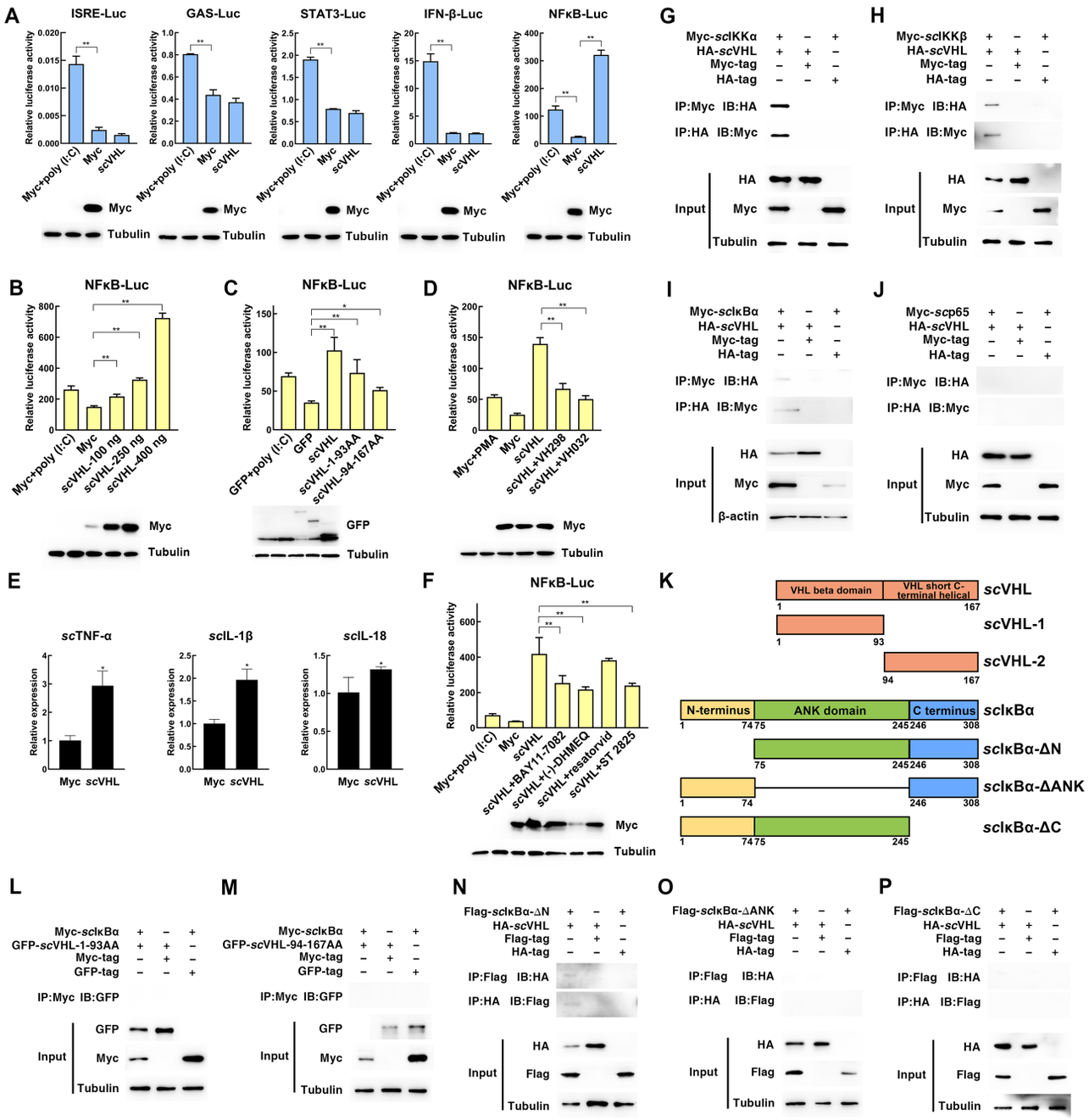

Figure 2 *sc*VHL activated the NF-κB signaling pathway through interactions with *sc*IKKα, *sc*IKKβ, and *sc*IκBα

A: *sc*VHL activates the NF-κB promoter. Promoter plasmids ISRE-Luc, cGAS-Luc, STAT3-Luc, IFNβ-Luc, and NF-κB-Luc were co-transfected with *sc*VHL and pRL-TK into FHM cells, with luciferase activity assessed after 24 h. B: Dose-dependent induction of NF-κB promoter by scVHL overexpression and stimulation by different scVHL sections, as well as inhibition by VHL inhibitors. NF-κB promoter was co-transfected with different doses of *sc*VHL vector in FHM cells, with luciferase activity then detected. C: Luciferase analysis of different sections with overexpression of NF-κB promoter and *sc*VHL. D: Luciferase analysis of overexpression of *sc*VHL and NF-κB promoter following the addition of DMSO, VH298, and VH032 to the medium. E: RT-qPCR was used to measure the expression levels of *scTNF-α* and *scIL-1β* after overexpressing *sc*VHL. F: Identification of activity site of the NF-κB promoter upon *sc*VHL overexpression. FHM cells were co-transfected with NF-κB promoter and *sc*VHL, followed by the addition of BAY-11-7082, -(-)DHMEQ, resatorvid, and ST2825, with luciferase activity then detected. G–J: Interaction of *sc*VHL with *sc*IKKα (G), *sc*IKKβ (H), *sc*IκBα (I), and *sc*P65 (J). FHM cells were transfected with pCMV-HA-*sc*VHL or empty vector and pCMV-Myc-*sc*IKKα, pCMV-Myc-*sc*IKKβ, pCMV-Myc-*sc*IκBα, and pCMV-Myc-*sc*p65 plasmids. Co-immunoprecipitation and western blotting analyses were used for detection. IB, immunoblotting; IP, immunoprecipitation. K–P: Interaction sites between *sc*IκBα and *sc*VHL. K: Organization of *sc*VHL and various *sc*IκBα domains. Interactions between *sc*IκBα and *sc*VHL-1 (L) or *sc*VHL-2 (M). Interactions between *sc*VHL and *sc*IκBα-ΔN (N), *sc*IκBα-ΔANK (O), and *sc*IκBα-ΔC (P). *: $P<0.05$; **: $P<0.01$.

aa and 246–308 aa), and *sc*IκBα-ΔC (1–245 aa) (Figure 2K). Co-IP assay showed no interaction bands in the groups co-overexpressing *sc*IκBα with either *sc*VHL-1 (1–93 aa) or *sc*VHL-2 (94–167 aa) (Figure 2L, M). Full-length *sc*VHL interacted with *sc*IκBα-ΔN, while no bands were detected in the *sc*VHL and *sc*IκBα-ΔANK or *sc*IκBα-ΔC co-expression

groups (Figure 2N–P). These results suggest that the ANK and C-terminal domains of *sc*IκBα are the primary interaction regions for *sc*VHL, and both the α and β domains are required for binding to *sc*IκBα. These findings indicate that *sc*VHL activates the NF-κB signaling pathway through interactions with *sc*IKKα, *sc*IKKβ, and *sc*IκBα.

*Sc*VHL did not affect *sc*IKKα, *sc*IKKβ, and *sc*IκBα degradation

Given the well-established role of VHL as an E3 ubiquitin ligand that facilitates proteasomal degradation, we next investigated whether *sc*VHL mediates the proteasomal degradation of *sc*IKKα, *sc*IKKβ, and *sc*IκBα. Cells were cotransfected with Myc-*sc*IKKα, Myc-*sc*IKKβ, or Myc-*sc*IκBα along with HA-*sc*VHL or empty vector. After 24 h of transfection, the cells were treated with the protein synthesis inhibitor cycloheximide (CHX, 100 μmol/L) or a combination of CHX and the proteasome inhibitor MG132 (20 μmol/L) for 0, 2, 4, and 8 h. The cells were then harvested and lysed for western blot analysis. As shown in Figure 3A–C, the protein levels of *sc*IKKα and *sc*IKKβ remained unchanged regardless of co-expression with *sc*VHL. In addition, while the *sc*IκBα protein was degraded over time, the degradation rate did not differ between cells overexpressing *sc*VHL and those expressing the empty vector. Treatment with MG132 slowed the degradation rate of *sc*IκBα, but there was no change in cells overexpressing *sc*VHL. Moreover, when cells were co-overexpressed with varying doses of the *sc*VHL vector and *sc*IKKα/*sc*IKKβ/*sc*IκBα, the levels of these target proteins remained unchanged (Figure 3D–F). These results suggest that *sc*VHL does not affect the degradation of *sc*IKKα, *sc*IKKβ, and *sc*IκBα.

To further explore how *sc*VHL regulates NF-κB activation through its interaction with *sc*IκBα, cells were co-transfected with *sc*IκBα, *sc*p65, and different doses of the *sc*VHL vector. Co-IP assays were conducted to examine the interaction between *sc*IκBα and *sc*p65 in the presence of different doses of *sc*VHL. Results showed that different doses of *sc*VHL did not affect the binding between *sc*IκBα and *sc*p65 (Figure 3G), indicating that *sc*VHL does not act as a competitive binding protein in the interaction between *sc*IκBα and *sc*p65.

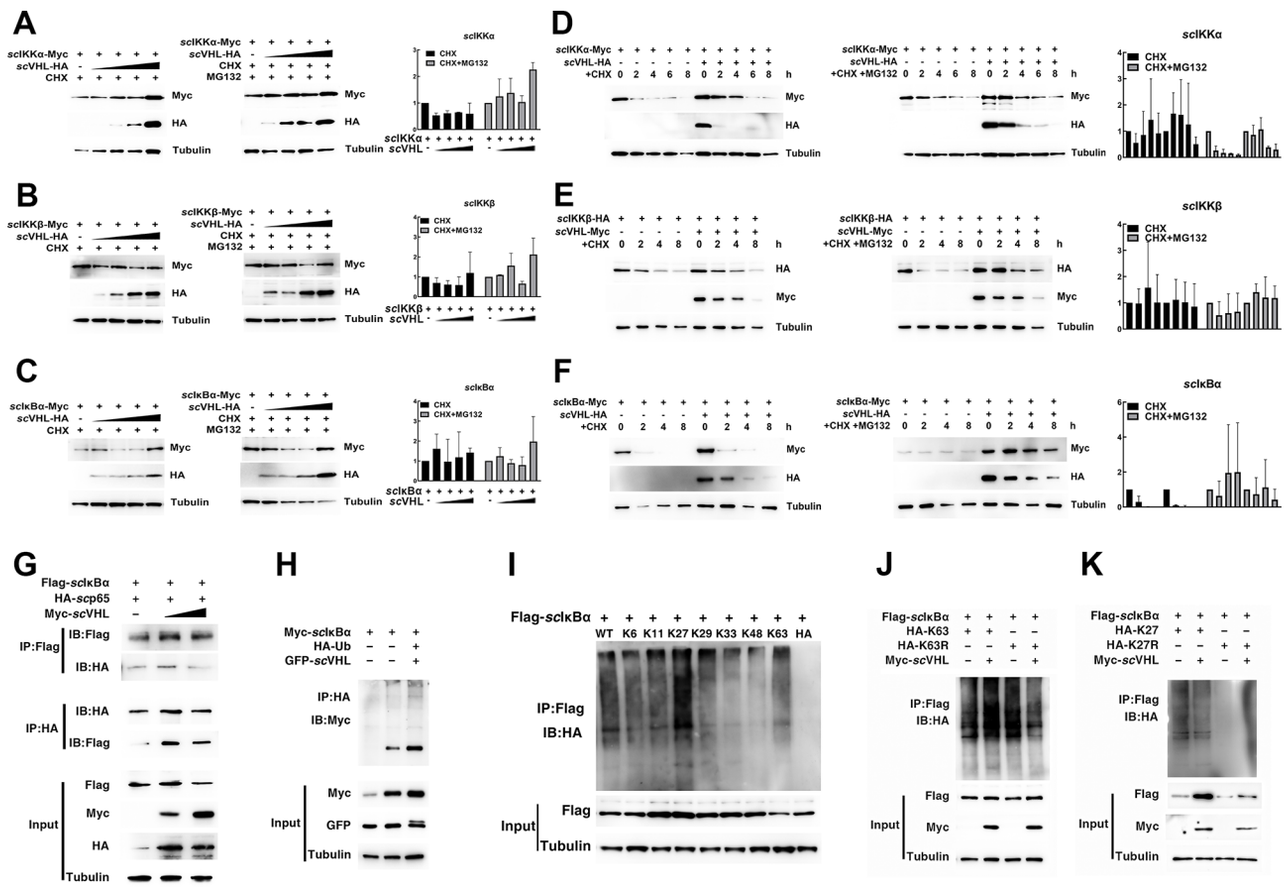

Figure 3 *sc*VHL regulated the NF-κB signaling pathway by promoting *sc*IκBα K63 ubiquitination

A–C: Overexpression of different doses of *sc*VHL did not affect the stabilization of *sc*IKKα (A), *sc*IKKβ (B), or *sc*IκBα (C) in the presence or absence of CHX and MG132. FHM cells were transfected with indicated plasmids for 24 h, treated with CHX or MG132, and harvested for western blotting. D–F: Stabilization of *sc*IKKα (D), *sc*IKKβ (E), and *sc*IκBα (F) did not change with or without *sc*VHL at different time points. FHM cells were transfected with indicated plasmids for 24 h, treated with CHX or MG132, and analyzed by western blotting at different time points. Ratio of gray value of each target protein to tubulin, average values were calculated for graph. G: *sc*VHL did not interfere with the interaction of *sc*IκBα and *sc*p65. FHM cells were co-transfected with *sc*IκBα, *sc*p65, and different doses of *sc*VHL or empty vector, followed by Co-IP analysis. H: *sc*VHL catalyzed polyubiquitination of *sc*IκBα. FHM cells were co-transfected with *sc*IκBα, *sc*VHL, and Ub-wt for 24 h, then harvested for Co-IP analysis. I: Identification of *sc*IκBα ubiquitination type. FHM cells were co-transfected with *sc*IκBα and Ub-wt, K6, K11, K27, K29, K33, K48, K64, or empty plasmid, then lysed for Co-IP analysis with anti-Flag antibodies as indicated. J, K: *sc*VHL catalyzed K63- but not K27-linked polyubiquitination of *sc*IκBα. FHM cells were co-transfected with *sc*IκBα, *sc*VHL, K27 or K27R (J), K63, or K63R (K) for 24 h, then harvested for Co-IP analysis.

*Sc*VHL markedly enhanced K63-linked ubiquitination of *sc*IκBα

VHL functions as a target recruitment subunit within the E3 ubiquitin ligase complex, facilitating ubiquitination (Tanimoto et al., 2000). To examine whether the interaction between *sc*VHL and *sc*IκBα affects *sc*IκBα ubiquitination, cells were co-transfected with *sc*VHL, *sc*IκBα, and Ub-wt vectors, followed by Co-IP analysis. Results showed a significant increase in *sc*IκBα ubiquitination in the presence of *sc*VHL (Figure 3H). To identify the specific types of *sc*IκBα ubiquitination, cells were transfected with Myc-*sc*IκBα and various ubiquitin constructs, including Ub-wt, K6, K11, K27, K29, K33, K48, K63, and empty vector. Co-IP assays revealed that *sc*IκBα underwent K27- and K63-linked ubiquitination in normal cells (Figure 3I). To further confirm the role of *sc*VHL in promoting *sc*IκBα ubiquitination, cells were co-transfected with *sc*IκBα, *sc*VHL, and either Ub-K27/K27R or Ub-K63/K63R. Co-IP analysis showed that *sc*VHL specifically induced K63-linked ubiquitination of *sc*IκBα, but not K27-linked ubiquitination (Figure 3J, K). In addition, *sc*VHL did not regulate other types of *sc*IκBα ubiquitination (data not shown). These findings indicate that *sc*VHL activates the NF-κB signaling pathway by interacting with *sc*IκBα and enhancing its K63-linked ubiquitination.

Activated NF-κB signaling pathway positively regulates MRV infections

The NF-κB signaling pathway is a key regulator of innate and adaptive immunity and the inflammatory response, with many viruses exploiting NF-κB to enhance their replication (Deng et al., 2018; Santoro et al., 2003). To investigate the involvement of the NF-κB signaling pathway in the response to MRV infection, RT-qPCR was employed to measure the transcription levels of NF-κB-related genes at various time points post-infection. As shown in Figure 4A, genes associated with the NF-κB signaling pathway (*scIKKα*, *scIKKβ*, *scIκBα*, *scp65*, *scp100*, *scp105*, *scRel B*, *scC-Rel*, *scMyD88*, *scTNF-α*, *scIL-1β*, and *scIL-18*) responded to MRV infection. The mRNA levels of *scIKKα*, *scp65*, *scp100*, *scC-Rel*, *scTNF-α*, *scIL-1β*, and *scIL-18* exhibited a rapid increase at 24 h post-infection, peaking at 36 h. The *scIKKβ* and *scMyD88* genes were highly expressed at 24 h post-infection and remained elevated throughout the infection period. The expression levels of *scIκBα* and *scp105* continued to increase during viral infection, while *scRelB* expression only responded to MRV infection at 12 h post-infection. These observations suggest that the NF-κB signaling pathway is actively involved in the host response to MRV infection.

To verify whether MRV infection is influenced by NF-κB activity, the transcription levels of the viral gene *MRV-MCP*, viral genomic copies, and viral titers were evaluated in cells overexpressing *sc*IKKα, *sc*IKKβ, *sc*IκBα, *sc*p65, *sc*p100, *sc*P105, *sc*C-Rel, *sc*Rel B, *sc*MyD88, or *sc*TNF-α after MRV infection. As shown in Figure 4B–I, *MRV-MCP* transcription and viral genome copies were significantly increased after cells were overexpressed with *sc*IKKα, *sc*IKKβ, *sc*p65, *sc*MyD88, *sc*TNF-α, *sc*Rel B, *sc*p100, and *sc*p105 compared to the control group. Additionally, at 72 h post-infection, the $TCID_{50}$ values were notably higher in cells overexpressing *sc*IKKα, scMyD88, *sc*TNF-α, *sc*Rel B, scp100, and *sc*p105, while no significant changes were observed in cells overexpressing *sc*IKKβ and *sc*p65 (Figure 4B–I). In contrast, cells overexpressing *sc*IκBα and *sc*C-Rel showed a significant decrease in *MRV-MCP* gene expression, viral genomic copies, and viral titers compared to the control (Figure 4J, K). To confirm these results, an RNAi assay was performed to knockdown the *sc*IκBα mRNA levels. As shown in Figure 4L–N, knockdown of *sc*IκBα led to a marked increase *MRV-MCP* expression, viral genomic copies, and viral titers compared to the control group. These results indicate that MRV infection activates the NF-κB signaling pathway, and this activation promotes MRV infection.

*Sc*VHL promoted MRV replication through NF-κB activation

To explore the role of *sc*VHL in MRV infection, cells transfected with *sc*VHL vectors were infected with MRV, with *MRV-MCP* gene expression, viral genomic copies, and viral titers then measured at 24 h and 48 h post-infection. As shown in Figure 5A, viral mRNA levels (*MRV-MCP*, *MRV-ICP18*, and *MRV DNA polymerase*) were significantly up-regulated at 24 h post-infection. Additionally, viral genomic copies and viral titers were markedly higher compared to the control group (Figure 5B, C). Similar experiments conducted in FHM cells confirmed these findings, with increased levels of viral mRNAs, viral genomic copies, and viral titers observed in the *sc*VHL overexpression group (Figure 5D–F). These results suggest that *sc*VHL is beneficial for MRV replication.

To explore the role of *sc*VHL in MRV replication, siRNA and inhibitors were used. Results showed that the levels of viral mRNAs, viral genomic copies, and viral titers were significantly up-regulated in the *sc*VHL knockdown group compared to the control group (Figure 5G–I). The levels of viral mRNA (*MRV-MCP*, *MRV-ICP18* and *MRV DNA polymerase*) and viral genomic copies were significantly reduced after treatment with VH298 and VH032 compared to the controls treated with DMSO (Figure 5J–L). These results suggest that *sc*VHL promotes MRV replication through the activation of the NF-κB signaling pathway.

DISCUSSION

First identified in 1993, VHL has been extensively studied as an E3 ligase involved in the regulation of the HIF-1 signaling pathway (Gossage et al., 2015). In addition to its role in HIF-1 regulation, pVHL participates in various physiological processes, with mutation and inactivation of pVHL leading to severe diseases, such as kidney cancer (Kaelin, 2017; Kondo et al., 2002). Research has primarily focused on $VHL^{-/-}$ zebrafish as a model for studying embryonic lethality in mice (Santhakumar et al., 2012; Van Rooijen et al., 2011). Thus, research on VHL function in teleost fish remains limited. In this study, *sc*VHL was found to positively regulate the NF-κB signaling pathway in mandarin fish, presenting a distinct role compared to its function in humans. Furthermore, *sc*VHL was shown to bind to *sc*IKKα/*sc*IKKβ and *sc*IκBα without affecting their protein expression levels. Notably, *sc*IκBα was identified as a novel target of *sc*VHL in NF-κB regulation. Acting as an E3 ubiquitin ligase, *sc*VHL did not facilitate the protein degradation of *sc*IκBα but promoted its K63-linked ubiquitination. These observations indicate that *sc*VHL positively regulates the NF-κB signaling pathway by promoting NF-κB K63-linked ubiquitination. Few studies have reported on the types of IκBα ubiquitination, and the regulation of IκBα by pVHL warrants further exploration. This study provides novel insight into the mechanisms by which VHL regulates the NF-κB signaling pathway.

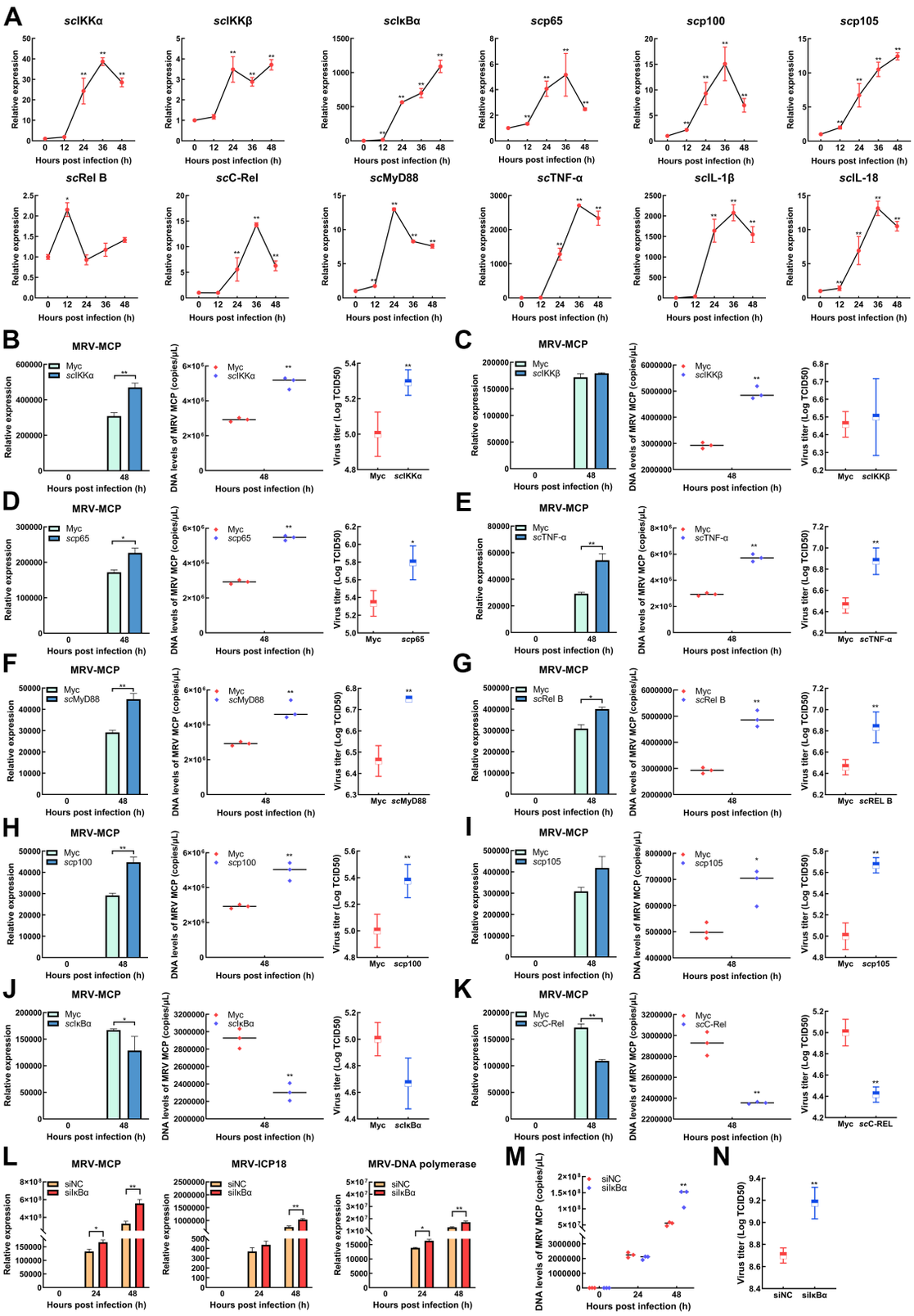

Figure 4 NF-κB signaling pathway activation promoted MRV transcription and replication

A: Expression levels of *scIKKα*, *scIKKβ*, *scIκBα*, *scp65*, *scp100*, *scp105*, *scRel B*, *scC-rel*, *scMyD88*, *scTNF-α*, *scIL-1β*, and *scIL-18* after MRV infection. B–K: NF-κB signaling pathway genes regulated MRV infectivity. FHM cells were overexpressed with *sc*IKKα (B), *sc*IKKβ (C), *sc*p65 (D), *sc*TNF-α (E), *sc*MyD88 (F), *sc*Rel B (G), *sc*p100 (H), *sc*IκBα (I), *sc*C-rel (J), and *sc*p105 (K), with empty vector used as a control. MRV cells were infected after 24 h of transfection, RT-qPCR and qPCR were used to analyze the mRNA and DNA levels of *MRV-MCP* at 48 h postinfection. Viral titers of MRV were detected by $TCID_{50}$ at 72 h post-infection. L–N: Knockdown of *sc*IκBα promoted MRV replication. siRNAs were used to knockdown *sc*IκBα expression in MFF-1 cells. RT-qPCR and qPCR were used to analyze the mRNA and DNA levels of *MRV-MCP* at different times after MRV infection. Viral titers of MRV were detected by $TCID_{50}$ at 72 h post-infection. *: $P<0.05$; **: $P<0.01$.

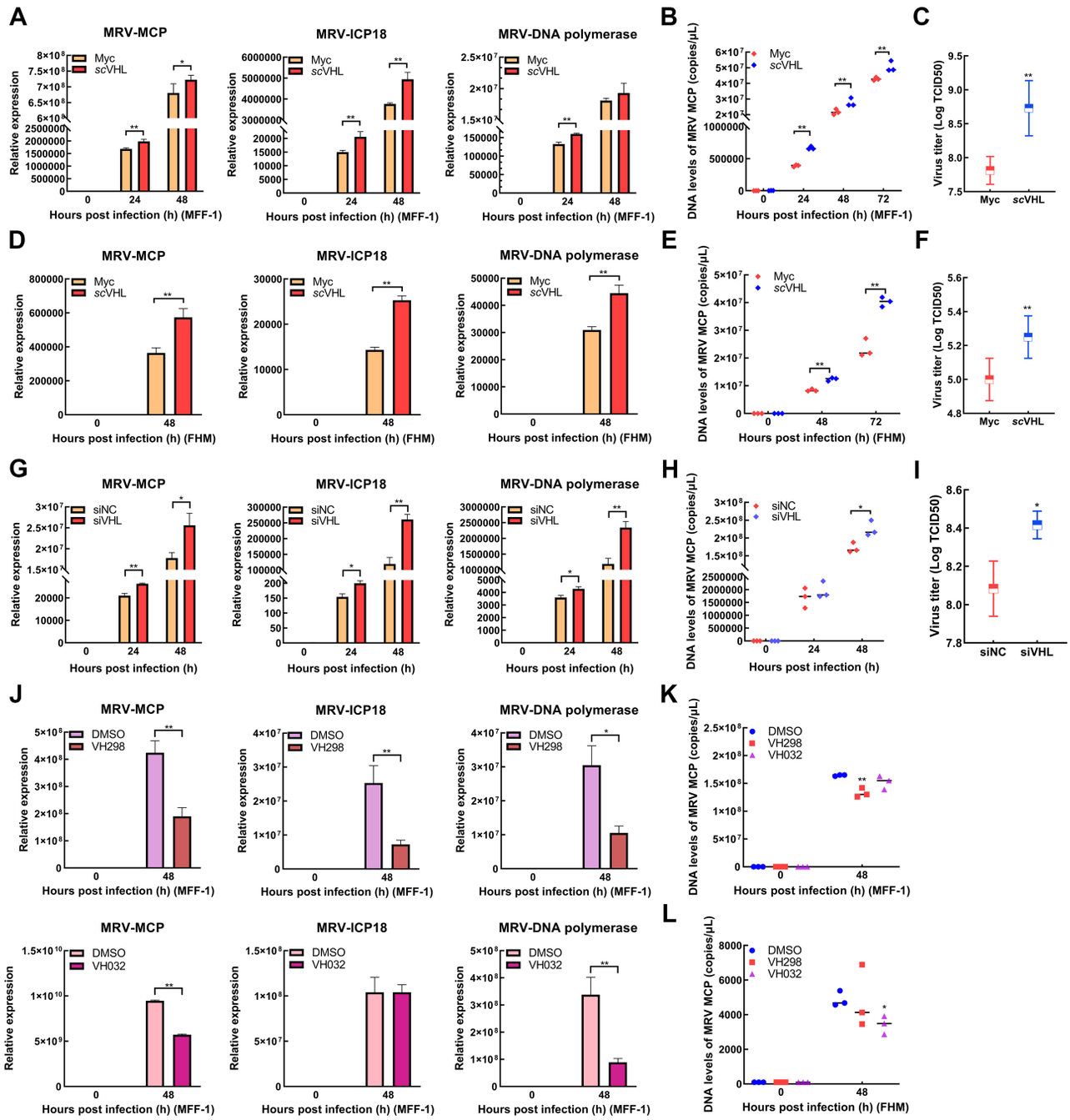

Figure 5 *sc*VHL activated the NF-κB pathway and enhanced MRV transcription and replication

A, B: Overexpression of *sc*VHL promoted MRV transcription and replication. *MRV-MCP*, *MRV-ICP018*, and *MRV-DNA polymerase* mRNA expression levels (A) and MRV-MCP DNA levels (B) were assessed in *sc*VHL-overexpressing MFF-1 cells by RT-qPCR and qPCR. C: Viral titers of MRV were detected by $TCID_{50}$ at 72 h postinfection. D–F: Overexpression of pCMV-Myc-scVHL or Myc-tag vector in FHM cells promoted MRV transcription and replication. mRNA levels (D), DNA copies (E), and viral titers (F) were detected in *sc*VHL-overexpressing FHM cells. G, H: Knockdown of VHL by VHL-siRNA inhibited MRV transcription and replication. MFF-1 cells were transfected with VHL-siRNA or siNC, MRV was infected at MOI=0.1, and cells were harvested at 0 h, 24 h, and 48 h post-infection for analysis. *MRV-MCP*, *MRV-ICP018*, and *MRV-DNA polymerase* mRNA expression levels (G) were assessed by RT-qPCR and MRV-MCP DNA levels (H) were assessed by qPCR. I: Viral titers of MRV were detected by $TCID_{50}$. J–L: VH298 and VH032 inhibited MRV transcription and replication. MFF-1 cells were treated with DMSO, VH298, and VH032 after MRV infection, and cells were harvested at 48 h post-infection. *MRV-MCP*, *MRV-ICP018*, and *MRV-DNA polymerase* mRNA expression levels (J) were assessed by RT-qPCR and MRV-MCP DNA levels (K) were assessed by qPCR in MFF-1 cells. L: MRV-MCP DNA levels were assessed by qPCR in FHM cells. *: $P<0.05$; **: $P<0.01$.

Although pVHL has been well studied due to its various functions related to VHL disease, further research into its role in viral infection is still needed. For example, pVHL negatively regulates severe acute respiratory syndrome (SARS) coronavirus replication by modulating the ubiquitination and stability of nsp16 (Yu et al., 2015), and also interacts with human immunodeficiency virus 1 (HIV-1) integrase, promoting its degradation (Mousnier et al., 2007). Furthermore, porcine reproductive and respiratory syndrome virus (PRRSV) nsp1β interacts with pVHL to impair the interaction between HIF-1α

and pVHL, hindering pVHL-mediated ubiquitination and degradation of HIF-1α, while pVHL stabilizes nsp1β via K63-linked ubiquitination, forming a positive feedback loop to further stabilize HIF-1α (Pang et al., 2022). pVHL also negatively regulates antiviral signaling by targeting MAVS (Du et al., 2015). In this study, *sc*VHL was identified as a multifunctional adaptor protein involved in regulating the NF-κB signaling pathway. NF-κB signaling pathway activation was hijacked by MRV to enhance viral replication. Overexpression of *sc*VHL promoted MRV replication by regulating the NF-κB signaling pathway. Additionally, *sc*VHL is a critical regulator of the HIF signal pathway, inhibiting its activation under normoxia. Under normoxic conditions, the HIF signal pathway is inhibited and *sc*VHL knockdown activates the HIF signal pathway. Under hypoxic conditions, the HIF signal pathway is activated and promotes viral replication through various mechanisms (He et al., 2022). Interestingly, knockdown of *sc*VHL up-regulated viral infection by regulating the HIF signal pathway. The role of *sc*VHL in MRV replication through multiple mechanisms should be further investigated. Our findings provide a foundation for future studies on the antiviral functions of VHL and its involvement in viral infections.

The NF-κB signaling pathway is a crucial component of the innate immune response, protecting the host against pathogen invasion by stimulating cytokine production (Santoro et al., 2003; Song & Li, 2021; Yu et al., 2020). However, many aquatic viruses can hijack or inhibit this pathway. For example, Singapore grouper iridovirus infection reduces NF-κB activity by up-regulating the expression of grouper *Epinephelus coioides* miR-122 (Sun et al., 2021). Infectious hematopoietic necrosis virus activates the NF-κB pathway in fish cells, while its L protein inhibits the pathway (Wu et al., 2017). The ORF124L protein of the infectious spleen and kidney necrosis virus interacts with *sc*IKKβ and inhibits the TNF-α-induced NF-κB signaling pathway (Guo et al., 2011). Additionally, the NV protein of the viral hemorrhagic septicemia virus inhibits NF-κB activation (Kim & Kim, 2013). The regulation of NF-κB during viral infection varies among different viruses. In this study, the NF-κB signaling pathway responded to MRV infection, with pathway activation further promoting MRV infection. Understanding the interactions between NF-κB and MRV infection could provide valuable insights into virus-host dynamics and inform strategies to combat MRV infections.

In conclusion, this study uncovered a novel molecular mechanism by which mandarin fish VHL activates the NF-κB signaling pathway and promotes MRV infection (Figure 6). Notably, MRV infection up-regulates *sc*VHL expression, which, in turn, interacts with *sc*IKKα, *sc*IKKβ, and *sc*IκBα to enhance *sc*IκBα K63-linked ubiquitination and NF-κB signaling, with activation of this pathway further promoting MRV replication. These findings contribute to our understanding of the interplay between host innate immune responses and viral immune evasion strategies, potentially informing future strategies to manage MRV disease outbreaks.

SUPPLEMENTARY DATA

Supplementary data to this article can be found online.

COMPETING INTERESTS

The authors declare that they have no competing interests.

AUTHORS' CONTRIBUTIONS

Z.M.L. performed the experiments. S.P.W. and J.G.H. provided the mandarin fish and MRV samples. Z.M.L., Q.Z., M.C.L., C.R.L., X.W.Q., W.H.L., and Y.Y. performed data and laboratory analyses. Z.M.L. and C.J.G. wrote the manuscript. C.J.G. and J.H. conceived the study. All authors read and approved the final version of the manuscript.

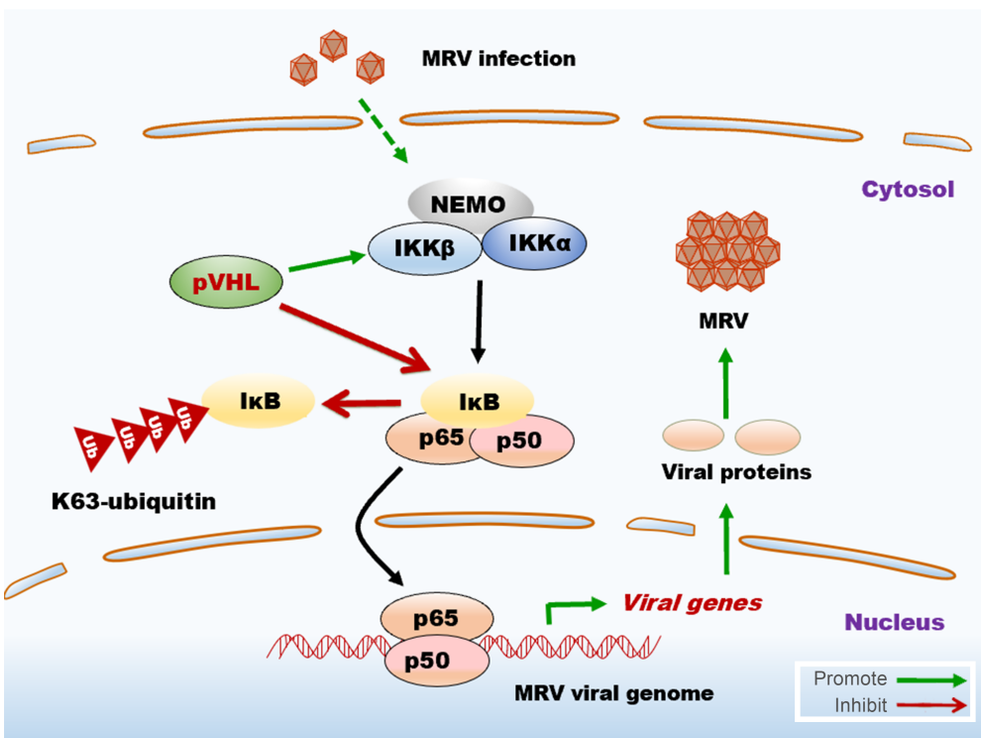

Figure 6 Model of interplay between VHL and IκBα in the regulation of MRV replication

MRV infection up-regulates VHL expression. VHL binds to IKKα, IKKβ, and IκBα to enhance IκBα K63-linked ubiquitination and activate NF-κB signaling. Activation of NF-κB promotes MRV replication. In general, the interaction between VHL and IκBα regulates MRV replication.

REFERENCES

An JB, Rettig MB. 2005. Mechanism of von Hippel-Lindau protein-mediated suppression of nuclear factor kappa B activity. *Molecular and Cellular Biology*, **25**(17): 7546–7556.

Bader HL, Hsu T. 2012. Systemic *VHL* gene functions and the VHL disease. *FEBS Letters*, **586**(11): 1562–1569.

Barontini M, Dahia PLM. 2010. VHL disease. *Best Practice & Research Clinical Endocrinology & Metabolism*, **24**(3): 401–413.

Deng LY, Zeng QR, Wang MS, et al. 2018. Suppression of NF-κB activity: a viral immune evasion mechanism. *Viruses*, **10**(8): 409.

Dong CF, Wang ZM, Weng SP, et al. 2017. Occurrence of a lethal ranavirus in hybrid mandarin (*Siniperca scherzeri*×*Siniperca chuatsi*) in Guangdong, South China. *Veterinary Microbiology*, **203**: 28–33.

Dong CF, Weng SP, Shi XJ, et al. 2008. Development of a mandarin fish *Siniperca chuatsi* fry cell line suitable for the study of infectious spleen and kidney necrosis virus (ISKNV). *Virus Research*, **135**(2): 273–281.

Du J, Zhang DW, Zhang W, et al. 2015. pVHL negatively regulates antiviral signaling by targeting MAVS for proteasomal degradation. *The Journal of Immunology*, **195**(4): 1782–1790.

Gossage L, Eisen T, Maher ER. 2015. VHL, the story of a tumour suppressor gene. *Nature Reviews Cancer*, **15**(1): 55–64.

Guo CJ, Chen WJ, Yuan LQ, et al. 2011. The viral ankyrin repeat protein (ORF124L) from infectious spleen and kidney necrosis virus attenuates nuclear factor-κB activation and interacts with IκB kinase *β*. *Journal of General Virology*, **92**(Pt 7): 1561–1570.

He J, Yu Y, Li ZM, et al. 2022. Hypoxia triggers the outbreak of infectious spleen and kidney necrosis virus disease through viral hypoxia response elements. *Virulence*, **13**(1): 714–726.

He JG, Wang SP, Zeng K, et al. 2000. Systemic disease caused by an iridovirus-like agent in cultured mandarinfish, *Siniperca chuatsi* (Basilewsky), in China. *Journal of Fish Diseases*, **23**(3): 219–222.

He JG, Wong SP, Huang ZJ, et al. 1998. Identification of outbreak and infectious diseases pathogen of *Siniperca chuatsi*. *Acta Scientiarum Naturalium Universitatis Sunyatseni*, **37**(5): 74–77. (in Chinese)

He S, Li L, Lv LY, et al. 2020. Mandarin fish (Sinipercidae) genomes provide insights into innate predatory feeding. *Communications Biology*, **3**(1): 361.

Hudler P, Urbancic M. 2022. The role of VHL in the development of von hippel-lindau disease and erythrocytosis. *Genes* (*Basel*), **13**(2): 362.

Kaelin Jr WG. 2017. The VHL tumor suppressor gene: insights into oxygen sensing and cancer. *Transactions of the American Clinical and Climatological Association*, **128**: 298–307.

Kim MS, Kim KH. 2013. The role of viral hemorrhagic septicemia virus (VHSV) NV gene in TNF-α- and VHSV infection-mediated NF-κB activation. *Fish & Shellfish Immunology*, **34**(5): 1315–1319.

Kondo K, Klco J, Nakamura E, et al. 2002. Inhibition of HIF is necessary for tumor suppression by the von Hippel-Lindau protein. *Cancer Cell*, **1**(3): 237–246.

Kumar S, Tamura K, Nei M. 1994. MEGA: Molecular Evolutionary Genetics Analysis software for microcomputers. *Bioinformatics*, **10**(2): 189–191.

Luo ZY, Zhan ZP, Qin XW, et al. 2023. Interaction of teleost fish TRPV4 with DEAD box RNA helicase 1 regulates iridovirus replication. *Journal of Virology*, **97**(6): e00495–23.

Mousnier A, Kubat N, Massias-Simon A, et al. 2007. von Hippel-Lindau binding protein 1-mediated degradation of integrase affects HIV-1 gene expression at a postintegration step. *Proceedings of the National Academy of Sciences of the United States of America*, **104**(34): 13615–13620.

Pang Y, Zhou YR, Wang YC, et al. 2022. Porcine reproductive and respiratory syndrome virus nsp1β stabilizes HIF-1α to enhance viral replication. *Microbiology Spectrum*, **10**(6): e03173–22.

Pantuck AJ, An JB, Liu HR, et al. 2010. NF-κB-dependent plasticity of the epithelial to mesenchymal transition induced by *Von Hippel-Lindau* inactivation in renal cell carcinomas. *Cancer Research*, **70**(2): 752–761.

Qin XW, Luo ZY, Pan WQ, et al. 2023. The interaction of mandarin fish DDX41 with STING evokes type i interferon responses inhibiting ranavirus replication. *Viruses*, **15**(1): 58.

Reed LJ, Muench H. 1938. A simple method of estimating fifty per cent endpoints. *American Journal of Epidemiology*, **27**(3): 493–497.

Santhakumar K, Judson EC, Elks PM, et al. 2012. A zebrafish model to study and therapeutically manipulate hypoxia signaling in tumorigenesis. *Cancer Research*, **72**(16): 4017–4027.

Santoro MG, Rossi A, Amici C. 2003. NF-κB and virus infection: who controls whom. *The EMBO Journal*, **22**(11): 2552–2560.

Song K, Li ST. 2021. The role of ubiquitination in NF-κB signaling during virus infection. *Viruses*, **13**(2): 145.

Spirina LV, Kondakova IV, Yurmazov ZA, et al. 2019. VHL expression in kidney cancer: relation to metastasis development, transcription and growth factors and component of akt/m-TOR signaling pathway. *Bulletin of Experimental Biology and Medicine*, **167**(5): 671–675.

Sun HY, Su YL, Li PH, et al. 2021. The roles of *Epinephelus coioides* miR-122 in SGIV infection and replication. *Marine Biotechnology*, **23**(2): 294–307.

Tanimoto K, Makino Y, Pereira T, et al. 2000. Mechanism of regulation of the hypoxia-inducible factor-1α by the von Hippel-Lindau tumor suppressor protein. *The EMBO Journal*, **19**(16): 4298–4309.

Van Rooijen E, Santhakumar K, Logister I, et al. 2011. A zebrafish model for VHL and hypoxia signaling. *Methods in Cell Biology*, **105**: 163–190.

Wang YX, Zhao WT, Gao Q, et al. 2016. pVHL mediates K63-linked ubiquitination of IKKβ, leading to IKKβ inactivation. *Cancer Letters*, **383**(1): 1–8.

Wu Y, Guo MT, Hua XJ, et al. 2017. The role of infectious hematopoietic necrosis virus (IHNV) proteins in the modulation of NF-κB pathway during IHNV infection. *Fish & Shellfish Immunology*, **63**: 500–506.

Yu H, Lin LB, Zhang ZQ, et al. 2020. Targeting NF-κB pathway for the therapy of diseases: mechanism and clinical study. *Signal Transduction and Targeted Therapy*, **5**(1): 209.

Yu X, Chen SL, Hou PP, et al. 2015. VHL negatively regulates SARS coronavirus replication by modulating nsp16 ubiquitination and stability. *Biochemical and Biophysical Research Communications*, **459**(2): 270–276.

Zeng RY, Pan WQ, Lin YF, et al. 2021. Development of a gene-deleted live attenuated candidate vaccine against fish virus (ISKNV) with low pathogenicity and high protection. *iScience*, **24**(7): 102750.

Zhang WF, Duan C, Zhang HT, et al. 2020. Widespread outbreaks of the emerging mandarinfish ranavirus (MRV) both in natural and ISKNV-FKC vaccinated mandarinfish *Siniperca chuatsi* in Guangdong, South China, 2017. *Aquaculture*, **520**: 734989.